

Elastic and inelastic scattering

1 Introduction

Elastic scattering of radioactive nuclei is also sensitive to their matter distribution. This is due to the dependence of the optical potential on the matter distribution, as is easily implied in the “ $t\rho\rho$ ” approximation

The scattering amplitude is given in terms of the scattered wave, $\psi_{\mathbf{r}}^+(\mathbf{r})$, by

$$f(\theta) = -\frac{\mu}{2\pi\hbar^2} \int e^{-i\mathbf{k}'\cdot\mathbf{r}} U(\mathbf{r})\psi_{\mathbf{k}}^+(\mathbf{r})d^3r \quad (1)$$

A simple approximation is obtained if we replace $\psi_{\mathbf{k}}^+$ by the plane wave, $e^{i\mathbf{k}\cdot\mathbf{r}}$, i.e.,

$$f_{BA}(\theta) = -\frac{\mu}{2\pi\hbar^2} \int e^{-i\mathbf{k}'\cdot\mathbf{r}} U(\mathbf{r}) e^{i\mathbf{k}\cdot\mathbf{r}} d^3r \quad (2)$$

This is known as the *Born-approximation*. Rearranged slightly this becomes

$$f_{BA}(\theta) = -\frac{\mu}{2\pi\hbar^2} \int e^{i\mathbf{q}\cdot\mathbf{r}} U(\mathbf{r})d^3r \quad (3)$$

which we recognize as the Fourier transform of the potential evaluated at $\mathbf{q} = \mathbf{k} - \mathbf{k}'$. Here \mathbf{q} is the change in momentum of the scattered particle. This momentum, \mathbf{q} , is transferred to the target and reappears as the recoil of the target. In terms of the scattering angle $q^2 = 2k^2 \sin^2(\theta/2)$. Thus, in this approximation, by measuring $f(\theta)$ one tests U , which by its way is related to the matter density. We will assess the theoretical tools which allow to cross the bridge from elastic scattering measurements to the information on the matter densities.

2 The distorted wave Born approximation

A more sophisticated version of the Born approximation is the distorted wave Born approximation. Suppose the potential U can be written as the sum of two terms, $U = U_1 + U_2$, and suppose we know or can easily obtain the scattering solution for U_1 ,

$$\{\nabla^2 + k^2 - U_1(\mathbf{r})\} \chi_{\mathbf{k}}^{\pm}(\mathbf{r}) = 0 \quad (4)$$

where $k^2 = 2\mu E/\hbar^2$. We use the notation

$$H_1 = H_0 + U_1, \quad H = H_1 + U_2 \quad (5)$$

and the Green's function formalism,

$$G_1^{\pm} = \frac{1}{E - H_1 \pm i\eta}, \quad G^{\pm} = \frac{1}{E - H \pm i\eta} \quad (6)$$

so that 4 can be written as

$$(E - H_1)\chi^{\pm} = 0 \quad (7)$$

and χ^\pm can be expressed in terms of plane waves states using Eq. ???. We get

$$\chi^\pm = \phi + G_0^\pm U_1 \chi^\pm, \quad \text{where } G_0 = \frac{1}{E - H_0 \pm i\eta}. \quad (8)$$

The relation between G_1 and G_0 can be determined by using

$$\frac{1}{A} - \frac{1}{B} = \frac{1}{B}(B - A) \frac{1}{A} \quad (9)$$

which is true for operators as well as for numbers. Hence, if $A = E - H_1 \pm i\eta$ and $B = E - H_0 \pm i\eta$ we find

$$G_1^\pm = G_0^\pm + G_0^\pm U_1 G_1^\pm \quad (10)$$

and reversing the definitions of A and B one find

$$G_0^\pm = G_1^\pm - G_1^\pm U_1 G_0^\pm \quad (11)$$

Substituting Eq. 11 into Eq. 8 one gets

$$\chi^\pm = \phi + G_1^\pm U_1 (\chi^\pm - G_0^\pm U_1 \chi^\pm) = \phi + G_1^\pm U_1 \phi \quad (12)$$

The solution of the complete problem with the potentials $U_1 + U_2$ obeys the equation

$$(E - H)\chi^\pm = 0 \quad (13)$$

and can be expressed again in terms of χ^\pm , by using Eqs. 8 and 12

$$\psi^\pm = \chi^\pm + G^\pm U_2 \chi^\pm = \chi^\pm + G_1^\pm U_2^\pm \psi^\pm \quad (14)$$

The transition matrix element is given by

$$\begin{aligned} T_{fi} &= \langle \phi | U_1 + U_2 | \psi^+ \rangle = \langle \phi | U_1 | \chi^+ \rangle + \langle \phi | U_1 G_1^+ U_2 | \psi^+ \rangle \\ &\quad + \langle \phi | U_2 | \chi^+ \rangle + \langle \phi | U_2 G_1^+ U_2 | \psi^+ \rangle \end{aligned}$$

where we have used Eq. 14. Now, since $G_0(\mathbf{r}, \mathbf{r}')$ is symmetric in \mathbf{r} and \mathbf{r}' it follows that

$$G_0^-(\mathbf{r}, \mathbf{r}') = \langle \mathbf{r}' | G_0^- | \mathbf{r} \rangle = [\langle \mathbf{r} | G_0^+ | \mathbf{r}' \rangle]^+ \quad (15)$$

or, simply $G_0^- = (G_0^+)^+$.

Using Eqs. 15 and Eq. 12 we have

$$\langle \phi | U_1 G_1^+ U_2 | \psi^+ \rangle = \langle G_1^- U_1^+ \phi | U_2 | \psi^+ \rangle = \langle \chi^- | U_2 | \psi^+ \rangle - \langle \phi | U_2 | \psi^+ \rangle$$

and similarly, using equation 14,

$$\langle \phi | U_2 G_1^+ U_2 | \psi^+ \rangle = \langle \phi | U_2 | \psi^+ \rangle - \langle \phi | U_2 | \chi^+ \rangle$$

Thus, collecting terms the transition matrix element is given by

$$T_{fi} = \langle \phi | U_1 | \chi^+ \rangle + \langle \chi^- | U_2 | \psi^+ \rangle \quad (16a)$$

From Eq. 1 we see that

$$f(\theta) = -\frac{\mu}{2\pi\hbar^2} \langle \phi | U | \psi^+ \rangle \quad (17)$$

Thus the relationship between the transition matrix element and the scattering amplitude is

$$f(\theta) = -\frac{\mu}{2\pi\hbar^2} T_{if} \quad (18)$$

The result 18 can be written as

$$f(\theta) = f_1(\theta) - \frac{\mu}{2\pi\hbar^2} \int \chi_1^{(-)*}(\mathbf{k}', \mathbf{r}) U_2(\mathbf{r}) \psi^{(+)}(\mathbf{k}, \mathbf{r}) d^3r \quad (19)$$

where we use the indices 1 on χ to indicate that they are distorted waves generated by the potential U_1 . The DWBA amplitude is obtained by approximating ψ^+ by χ_1^+ ,

$$f_{\text{DWBA}}(\theta) = f_1(\theta) - \frac{\mu}{2\pi\hbar^2} \int \chi_1^{(-)*}(\mathbf{k}', \mathbf{r}) U_2(\mathbf{r}) \chi_1^{(+)}(\mathbf{k}, \mathbf{r}) d^3r \quad (20)$$

This approximation is good if U_2 is weak compared to U_1 , and is called the “*distorted-wave Born approximation*”. It is “Born” because it is first order in the potential U_2 but “distorted wave” because instead of using the plane waves as in Eq. 3 we used the distorted waves χ_1 which should be a better approximation to the exact solution.

This approximation can be generalized to inelastic scattering. In this case, U_1 (and hence f_1) is chosen to describe the elastic scattering (i.e. it is an optical potential), while U_2 is the interaction which induces the non-elastic transition. The validity of the DWBA then depends upon elastic scattering being the most important event which occurs when two nuclei collide so that inelastic events can be treated as perturbations. The corresponding inelastic scattering amplitude for a reaction $A(a, b)B$ has the form

$$f_{\text{DWBA}}^{\text{inel}}(\theta) = -\frac{\mu}{2\pi\hbar^2} \int \chi_\beta^{(-)*}(\mathbf{k}_\beta, \mathbf{r}_\beta) \langle b, B | U_2 | a, A \rangle \chi_\alpha^{(+)}(\mathbf{k}_\alpha, \mathbf{r}_\alpha) d^3r_\alpha d^3r_\beta. \quad (21)$$

We have used this result before.

Here χ_1 has been generalized to χ_α and χ_β . The function χ_α describes the elastic scattering in the $\alpha = a + A$ entrance channel arising from an optical potential U_α , while χ_β describes the elastic scattering in the $\beta = b + B$ exit channel arising from a potential U_β . The potential U_2 which describes the non-elastic transition depends upon the type of reaction and the model chosen to describe it.

Supplement A

3 Polarization potentials for reactions with halo nuclei

The mean effect of the coupling between the elastic channel and excited states is expressed by the optical potential [1]. Instead of deriving this potential from first principles, one frequently adopts a phenomenological approach, expressing it in terms of a few parameters. These parameters, which may have a weak energy and/or mass dependence, are then fitted to a set of scattering data. When, however, a few channels have strong influence on the elastic scattering, it is necessary to handle the coupling with these channels separately. One possible approach is to express such effects as a correction to the optical potential. If one is able to obtain this correction, usually known as a *polarization potential*, the calculation of the elastic and the reaction cross sections reduces to the simple task of solving a one-channel Schrödinger equation. This approach has been used in several situations (for a review see [2]), including the cases of rotational [3, 4, 5, 6] and vibrational excitations and that of transfer channels [7, 8].

In this Section we discuss the derivation of the polarization potential resulting from the coupling to states corresponding to the removal of a halo nucleon from radioactive beam projectiles. This potential has been calculated by Canto, Donangelo and Hussein [9] for high energy collisions with light targets. We refer to that reference for more details on the calculations.

Following the procedure introduced by H. Feshbach [1] for the derivation of the optical potential, one defines the projection operators

$$P = |\phi_0\rangle\langle\phi_0|; \quad Q = 1 - P, \quad (22)$$

where $\phi_0(x) \equiv \phi_0(x)$ represents the bound state of the halo system while Q is the projector onto states in the continuum. The polarization potential can then be written [9]

$$V_{pol}(\mathbf{r}, \mathbf{r}') = \langle \mathbf{r}; \phi_0 | V Q G^+ Q V | \phi_0; \mathbf{r}' \rangle, \quad (23)$$

where V is the coupling interaction and G^+ is the optical Green's operator. In order to evaluate Eq. 23, we write the projector Q in its spectral form

$$Q = \int |\phi_q\rangle\langle\phi_q| dq, \quad (24)$$

with q standing for the set of quantum numbers that characterize the continuum states.

With introduction of representations in the space or the relative coordinate r and with the assumption that the interaction V is local, the polarization potential can be put in the form

$$V(\mathbf{r}, \mathbf{r}') = \mathcal{F}(r) G^{(+)}(\mathbf{r}, \mathbf{r}') \mathcal{F}(r'), \quad (25)$$

with the scalar form factor

$$\mathcal{F}(r) = U(r) \left[\int \phi_0^2(x) u^2(x) dx \right]^{1/2}. \quad (26)$$

In the derivation of Eq. 26, the following assumptions have been made [9]:

- the energies of the relevant states ϕ_q of Eq. 24 are small as compared to the collision energy,
- the matrix element $\langle \phi_0 | V | \phi_0 \rangle$ is negligible,
- the coupling potential is separable in the form: $V(r, x) \approx U(r) u(x)$, where $U(r)$ is the real part of the halo nucleus-target optical potential and $u(x)$ is an internal excitation form factor [10].

Performing the partial waves expansion of the polarization potential and writing the ℓ -projected Green's function explicitly, one gets the ℓ -components of the polarization potential

$$V_\ell(r, r') = \mathcal{F}(r) \left[-\frac{2\mu}{\hbar^2 k} f_\ell(kr_<) h_\ell^{(+)}(kr_>) \right] \mathcal{F}(r'). \quad (27)$$

Above, $f_\ell(kr_<)$ and $h_\ell^{(+)}(kr_>)$ are respectively the regular and the outgoing solutions of the radial equation with the optical potential.

For practical applications, it is convenient to use the trivially equivalent local potential, defined as [3]

$$V_\ell^{pol}(r) = \frac{1}{f_\ell(kr)} \int V_\ell^{pol}(r, r') f_\ell(kr') dr', \quad (28)$$

and adopt the on-shell approximation for the Green's function [3]. This approximation amounts to replacing $h_\ell^{(+)} \rightarrow if_\ell$ and its validity has been discussed in details in [11]. It leads to a separable Green's function and the trivially equivalent local potential takes the form

$$V_\ell^{pol}(r) = -i \frac{2\mu}{\hbar^2 k} \mathcal{F}(r) |S_\ell^{(1)}| \int_0^\infty \mathcal{F}(r') F_\ell^2(kr') dr', \quad (29)$$

where $S_\ell^{(1)}$ is the ℓ -component of the optical S-matrix and $F_\ell(kr)$ is the regular Coulomb function [12]. To get Eq. (29), the authors of Ref. [9] have approximated the radial wave function as $f_\ell(kr) \simeq |S_\ell^{(1)}|^{1/2} F_\ell(kr)$.

In the r -region of interest for the neutron-removal process, only the tail of $U(r)$ is relevant. Therefore, the form factor can be written as

$$\mathcal{F}(r) = \mathcal{F}_0 e^{-r/\alpha}, \quad \text{with } \mathcal{F}_0 = C e^{R_0/\alpha} r. \quad (30)$$

In Eq. 30, C is a constant which can be obtained from Eq. 26, $R_0 = R_{11Li} + R_{target}$, and α is the diffusiveness associated to the optical potential $U(r)$. Replacing Eq. 30 into Eq. 29, one gets

$$V_\ell^{pol}(r) = -i W_0(\ell, E) e^{-r/\alpha}. \quad (31)$$

The strength $W_0(\ell, E)$ is given by

$$W_0(\ell, E) = \frac{|\mathcal{F}_0|^2}{E} |S_\ell^{(1)}| I_\ell(\eta, s), \quad (32)$$

in terms of the radial integral

$$I_\ell(\eta, s) = \int_0^\infty e^{-s\rho} F_\ell^2(\rho) d\rho, \quad (33)$$

where η is the Sommerfeld parameter and $s = 1/(k\alpha)$.

Using the asymptotic WKB approximation for $F_\ell(\rho)$,

$$F_\ell(\rho) \approx \left(1 - \frac{2\eta}{\rho} - \frac{\ell(\ell+1)}{\rho^2}\right)^{-1/4} \sin \left[\frac{\pi}{4} + \int_{\rho_0}^{\rho} \sqrt{1 - \frac{2\eta}{\rho} - \frac{\ell(\ell+1)}{\rho^2}} d\rho \right], \quad (34)$$

where $\rho \equiv kr$ and ρ_0 is the value of ρ calculated at the turning point of the Rutherford trajectory, one obtains

$$I_\ell(\eta, s) = \frac{e^{-\eta s}}{2s} [\eta s K_0(X) + X K_1(X)]. \quad (35)$$

In Eq. 35, $K_0(X)$ and $K_1(X)$ are modified Bessel functions with the argument

$$X = \eta s \sqrt{1 + \frac{\ell(\ell+1)}{\eta^2}}. \quad (36)$$

The variable X measures the distance of closest approach in a Rutherford trajectory, in units of α .

For a comparison with the results of [9], the high energy and large ℓ limit was investigated. In this limit the polarization potential of Eq. (31) was shown to be identical to that obtained within the eikonal approximation [9].

4 Elastic scattering of halo nuclei

Reactions with secondary beams have been studied at relatively high energies, $E_{\text{lab}} \gtrsim 30$ MeV/nucleon. The distorted waves can be approximated by eikonal waves. This is valid for small angle scattering. To see how this approximation works we consider first the scattering of stable nuclei. The scattering amplitude in the eikonal approximation is

$$f_{\text{el}}(\theta) = ik \int b db J_0(qb) [1 - e^{i\chi(b)}] \quad (37)$$

where

$$\chi(b) = \chi_C(b) + \chi_N(b), \quad \chi_N(b) = -\frac{1}{\hbar v} \int_{-\infty}^{\infty} dz U [\sqrt{b^2 + z^2}] \quad , \quad (38)$$

is the nuclear eikonal phase and $\chi_C(b)$ is the Coulomb eikonal phase appropriate for light nuclei.

In Figure 1(a) we show the data on the elastic scattering of ^{17}O projectiles with an energy of $E_{\text{lab}} = 84$ MeV/nucleon bombarding ^{208}Pb targets. Data are from Ref. [13].

The calculation is done using Eq. 37 together with the “ $t\rho\rho$ ” approximation with the parameters for σ_{NN}, α_{NN} . We see that the approximation works extremely well (solid line). It should be said however that this system is not very sensitive to the optical potential since it is dominated by Coulomb scattering. Note that the vertical

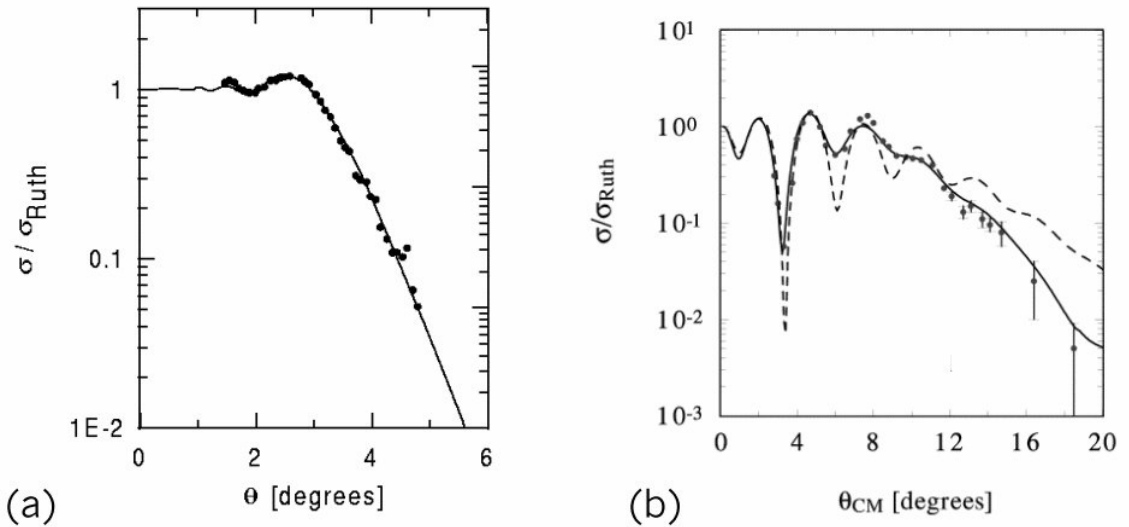


Figure 1 (a) Elastic scattering of ^{17}O projectiles with an energy of $E_{\text{lab}} = 84$ MeV/nucleon bombarding ^{208}Pb targets. (b) Elastic scattering data of $^{12}\text{C}+^{12}\text{C}$ at 84 MeV/nucleon.

scale is a ratio of the elastic scattering cross section and the Rutherford cross section. At $\theta \sim 3^\circ$ the cross section deviates from the Rutherford cross section and decreases rapidly. This is due to the strong absorption at small impact parameters. Any potential which is strongly absorptive (large imaginary part) at small impact parameters and rapidly decreases to zero at the strongly absorption radius will reproduce well the data. The “ $t\rho\rho$ ” potential is no exception to this.

A better test of the theory is provided by more “transparent” systems as, e.g., $^{12}\text{C}+^{12}\text{C}$. In Figure 1(b) we show the elastic scattering data of $^{12}\text{C}+^{12}\text{C}$ at 84 MeV/nucleon. The scattering is not dominated by Coulomb scattering as in the previous case. It is now much more sensitive to the optical potential chosen. The dashed curve is the one obtained with the “ $t\rho\rho$ ” approximation. We see that the agreement is quite good at forward angles, but it fails at large angles. However, this is not a failure of the eikonal approximation but of a good enough optical potential, which in this case was not provided by the “ $t\rho\rho$ ” approximation. To show this point we also plot in Figure 1(b) the result of an eikonal calculation [14], but with an adjusted optical potential (dashed line), the same one used in Ref. [13] with a full DWBA calculation. In fact, at these energies and for not a too large scattering angle ($\theta \lesssim 30^\circ$) the eikonal approximation works very well. The “ $t\rho\rho$ ” also gives reasonable results, as shown in Refs. [15] and [14]. We now turn to the elastic scattering with radioactive beams.

Due to the low intensity of radioactive beams ($\sim 10^3 - 10^4$ particles per second) the elastic scattering of radioactive beams were reported [16, 17] in few cases. To understand the motivation for such experiments let us decompose $f(\theta)$ into “near” and “far” side components. This is accomplished by first writing the

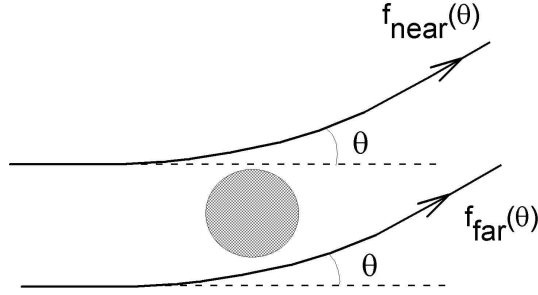


Figure 2 Near and far decomposition of the scattering amplitude.

Bessel function J_0 in Eq. 37 as

$$J_0(qb) = \frac{1}{2} \left[H_0^{(1)}(qb) + H_0^{(2)}(qb) \right] \quad (39)$$

where $H_0^{1(2)}(qb)$ is the Hankel function of order zero and first (second) type. Asymptotically, these functions behave as running waves. With that the amplitude $f(\theta)$ can be written as $f(\theta) = f_{\text{near}}(\theta) + f_{\text{far}}(\theta)$, where $f_{\text{near}}(\theta)$ [or $f_{\text{far}}(\theta)$] is given by Eq. 37 with $J_0(qb)$ replaced by $\frac{1}{2} H_0^{(2)}(qb)$ [or $\frac{1}{2} H_0^{(1)}(qb)$]. The function $H^{(2)}(qb)$ is more sensitive to large values of b than $H^{(1)}(qb)$ does.

This fact is mainly due to the Coulomb interaction. In the limit when $\chi_C(qb)$ is negligible and $\chi_N(qb)$ is pure imaginary (no refraction) it is easy to see that the following relation holds (from the properties of the $H_0^{1(2)}$ functions)

$$f_{\text{near}}(\theta) = -f_{\text{far}}^*(\theta) \quad (40)$$

The above results in an angular distribution, $f(\theta)$, that exhibits simple black-disk Fraunhofer diffraction patterns since the near and far amplitudes are equal in magnitude and interfere, as shown in Figure 2.

Back to Figure 1 we observe a small bump in the ratio-to-Rutherford cross section before the angular distribution goes down in magnitude. This is called by the *nuclear rainbow* effect. This is a situation characterized by the dominance of the far side component over the near side. In other words, as the impact parameter decreases the influence of the Coulomb interaction also diminishes and the nuclear force pushes the wave strongly (refracts strongly) to the other side of the nucleus interfering there with the other part of the wave.

At very small angles one always encounters the opposite situation, namely, $f_{\text{near}}/f_{\text{far}} \gg 1$, owing to the influence, on the angular region, of Coulomb repulsion which affects mostly f_{near} .

The motivation for the elastic scattering with radioactive beams can now be made clear. The elastic scattering of light systems as $^{12}\text{C} + ^{12}\text{C}$, $^{16}\text{O} + ^{12}\text{C}$ and $^{16}\text{O} + ^{16}\text{O}$ shows sufficient transparency for the cross sections to be dominated by far side scattering. It has been speculated that exotic nuclei like ^{11}Li would exhibit

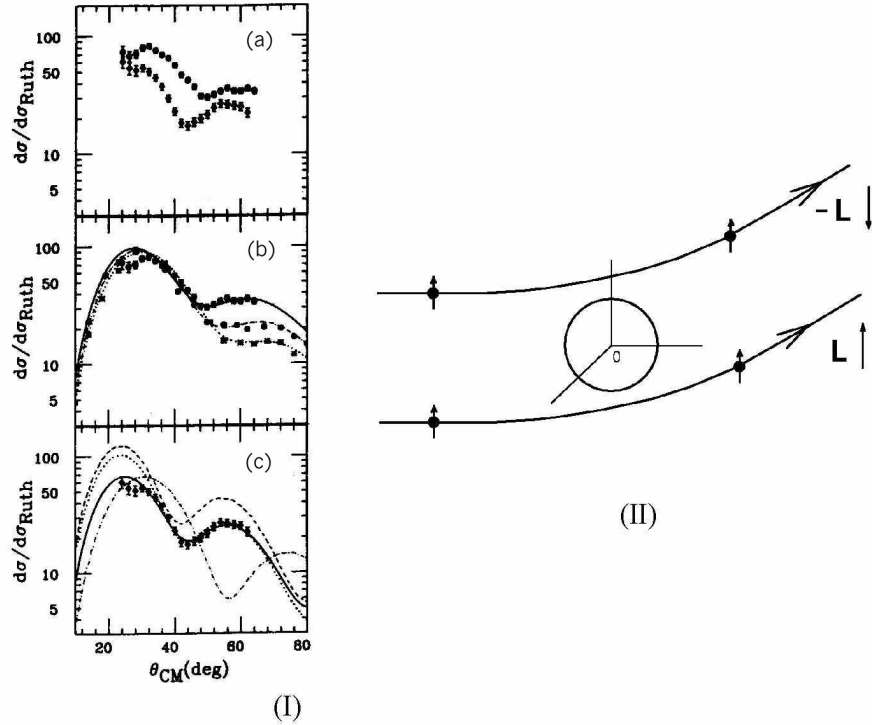


Figure 3 (I) Elastic scattering of protons on lithium isotopes at $E_{\text{lab}} = 62$ MeV, reported in ref. [18]. (a) Upper data points: $p + {}^{11}\text{Li}$. Lower data points: $p + {}^9\text{Li}$. (b) Upper data points: $p + {}^9\text{Li}$. Middle data points: $p + {}^7\text{Li}$. Lower data points: $p + {}^6\text{Li}$. (c) $p + {}^{11}\text{Li}$. (II) Sketch of spin-orbit effect on elastic scattering.

much stronger absorption because of the weak binding of the excess neutrons so that there would no longer be far-side dominance. Then the scattering would be more characteristic of the scattering by a black sphere for which the near side and far side amplitudes are equal at all angles and their interference produces marked diffractive oscillations. However, we shall show here that there are good reasons to believe that this is not so, and that the scattering is still dominated by refraction.

We first study the case of $p + {}^{11}\text{Li}$ elastic scattering. This has been measured and reported in Ref. [18] at $E_{\text{lab}} = 62$ MeV. The results are shown in Fig. 3(I-a) (upper data points) together with data for $p + {}^9\text{Li}$ at $E_{\text{lab}} = 60$ MeV (lower data points). What is shown is the ratio to the Rutherford cross section. Unfortunately, these $p + {}^9\text{Li}$ data are not purely elastic. Due to experimental difficulties possible inelastic scattering to the $(1/2^-; 2.69$ MeV) excited state in ${}^9\text{Li}$ could not be separated in the ${}^9\text{Li}$ data. It has been estimated that the inelastic contribution was not more than 30% of the total measured cross section [18].

One striking feature in the $p + {}^{11}\text{Li}$ angular distribution is observed; while the angle of diffraction minimum follows from the systematics, the cross section values are reduced as compared with those of the other isotopes. What is understood by

systematics here is that the diffraction angle is proportional to $\theta \sim \frac{1}{R}$. Since $R \sim A^{1/3}$, then $\theta \sim 1/A^{1/3}$, i.e., decreases with $\sim A^{1/3}$.

An eikonal calculation can be done, using 37 and a standard potential of the form

$$\begin{aligned}
 U_N(r) = & -V_R f_V(r) - iW_R f_W(r) + 4ia_I V_I \frac{d}{dr} f_W(r) \\
 & + 2 \left(\frac{\hbar}{m_\pi c} \right)^2 \frac{1}{r} \frac{d}{dr} [V_S f_S(r)] (\mathbf{1} \cdot \mathbf{s}) + V_{\text{coul.}}
 \end{aligned} \tag{41}$$

where

$$f_i(r) = 1 / \{1 + \exp[(r - R_i)/a_i]\} \tag{42}$$

for $i = V, W$ and S ; with $R_i = r_i A^{1/3}$. The first (second) term is the usual real (imaginary) part of the optical potential. The third term is peaked at the surface of the nucleus and is used to simulate a stronger absorption of the incoming nucleon at the surface of the nucleus. It is a correction due to the Pauli blocking effect. Since the momentum states of the nucleons are occupied in the nucleus, the incoming nucleon has no chance to scatter into those states. This has the effect of reducing the nucleon-nucleon cross section and consequently the absorption. At the nuclear surface the nucleons are not as densely packed and not as many momentum states are occupied. Therefore, nucleon-nucleon scattering is more effective, increasing the absorption. The third term is a small correction in general.

Nucleus	Set	Real				Imaginary				Spin-orbit			σ_R (mb)
		V_R	r_R	a_R	W_v	W_s	r_I	a_I	V_S	r_S	a_s		
${}^6\text{Li}$	A	35.96	1.13	0.69	6.63	3.20	1.10	0.68	5.9	0.68	0.63	235	
${}^7\text{Li}$	A	35.96	1.13	0.69	15.15	1.06	1.14	0.60	5.9	0.71	0.63	258	
${}^9\text{Li}$	A	35.96	1.13	0.69	18.78	0.00	1.06	0.64	5.9	0.76	0.63	298	
${}^{11}\text{Li}$	A	35.96	1.13	0.69	6.46	4.35	1.17	0.79	5.9	0.80	0.63	461	
	B	18.06	1.385	0.546	4.26	4.60	0.56	1.16	5.9	0.80	0.63	388	

Table 8.1 - Parameters for the real part of the central potential and for the imaginary party of the central potential. V_i and W_i are in MeV, and r_i and a_i are in fm.

The last term in Eq. 41 is a spin-orbit correction. It follows the same principles as the spin-orbit interaction in atoms. It causes interference between the scattering from opposite sides of the nucleus, as shown in Fig. 3(II) where a proton with spin up scatters from one and the other side of the nucleus. Since the angular momentum of the proton changes sign in one and the other case, the spin-orbit interaction also changes sign. The interference between these two situations leads to pronounced effects in the angular distribution.

The parameters used to describe the elastic scattering of several nuclei are shown in Table 8.1 [18]. These fits are shown in Fig. 3(I-b) together with the experimental data for ${}^6\text{Li}$, ${}^7\text{Li}$ and ${}^9\text{Li}$. In Fig. 3(I-c) several fits are shown which are

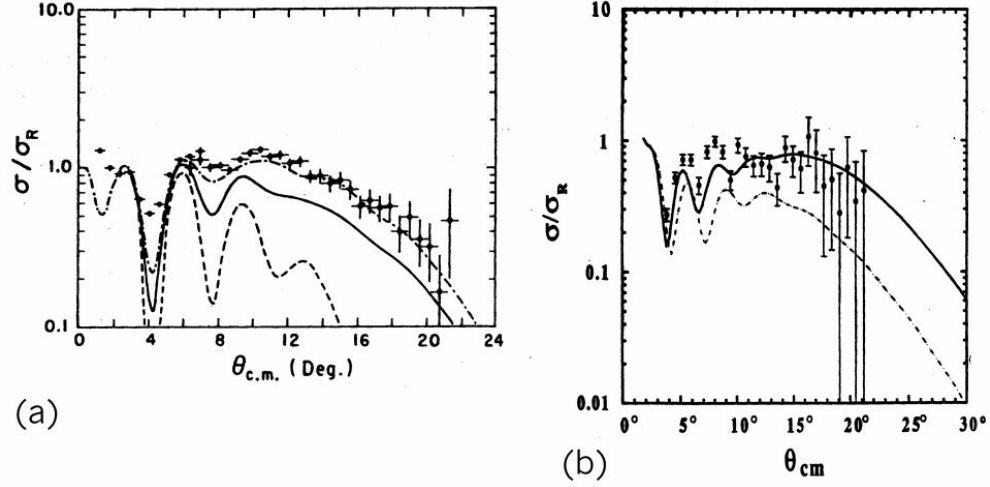


Figure 4 Elastic scattering of ^{11}Li by ^{12}C (a) and by ^{28}Si (b) as reported in Refs. [16, 17].

not worth the discussion, since they fail badly to reproduce the data. They have been generated with optical potentials based on the folding of the densities (e.g., the “ $t\rho\rho$ ”-potential). This shows that the relationship of matter densities and elastic scattering is not an easy task to accomplish. The solid curve is a fit obtained with the optical potential parameters in the last row of Table 3.1. A microscopic calculation using multiple nucleon-nucleon collisions [19] was also not able to reproduce the data [18].

In order to understand what is the reason for this disagreement we look back into Eq. 21. Elastic scattering occurs for $a = b$ and $A = B$. Let us assume that a represents ^{11}Li . we see that under the action of a small interaction a wavefunction is modified in lowest order to

$$|\psi'_n\rangle = |\psi_n\rangle + \sum_{m \neq n} \frac{\langle \psi_m | U | \psi_n \rangle}{E_n - E_m} |\psi_m\rangle \quad (43)$$

If we assume that $|\psi_n\rangle$ is the ground state this equation says that during the action of the potential U the wavefunction acquires small components from excited states. At the end of this process the wavefunction can return to its initial state again. The modification of the wavefunction during the action of the potential is called by “polarization”. It does not lead to an excitation but it has consequences.

This phenomenon can be described by a “*polarization potential*”, which is proportional to the second term of Eq. 43 (see Supplement A). In ^{11}Li there are no excited states. In this case, the sum in Eq. 43 has to be replaced by an integral over states in the continuum. It is believed that, since the binding energy of ^{11}Li , or ^{11}Be , is quite small, the strength* of this coupling to the states in the continuum is quite

*Not only $\langle 0 | U | \psi_{\text{cont.}} \rangle$, but also $E_{\text{cont.}} - E_0$ is small.

large [20]. A derivation of a polarization potential appropriate for the coupling to the states in the continuum of a halo nucleus is presented in Supplement A.

For nucleus-nucleus elastic scattering the theoretical description is in principle simpler since the surface and spin-orbit terms of the potential are absent. Elastic scattering of ${}^{11}\text{Li}$ by ${}^{12}\text{C}$ and ${}^{28}\text{Si}$ have been measured [16, 17]. The data were also contaminated by inelastic scattering. These are shown in Figs. 4 together with fits from numerical calculations with properly chosen optical potentials. The basic conclusion of these two works is that the optical potentials have to be of long range. But the scattering is still dominated by refraction, i.e., $f_{\text{far}}(\theta) \gg f_{\text{near}}(\theta)$ [22].

The elastic scattering data can be used to discriminate between different nuclear models for Borromean systems. A work along these lines was performed by Thompson and collaborators [23].

Supplement B

5 Vibrational (or deformed) potential model

The asymptotic form of the scattered wave for an unbound particle is

$$\phi_{\mathbf{k},\alpha}^{(\pm)} = \left[e^{i\mathbf{k}\cdot\mathbf{r}} + f_{\mathbf{k}}^{(\pm)}(\theta) \frac{e^{\pm ikr}}{r} \right] \chi_s \quad (44)$$

where χ_s is a spin-isospin wave function.

Assuming that a residual interaction U_{int} between the projectile and target exists and is weak we can use the DWBA result 21 for the inelastic amplitude. For a nuclear excitation $|0\rangle \rightarrow |\lambda\mu\rangle$, where $\lambda\mu$ is the final angular momentum (and projection), it is convenient to define

$$\langle \mathbf{k}_\lambda | T_{\lambda\mu} | \mathbf{k}_0 \rangle \equiv \langle \psi_{\lambda\mu} \phi_{\mathbf{k}_\lambda}^{(-)} | U_{\text{int}} | \psi_0 \phi_{\mathbf{k}_0}^{(+)} \rangle \quad (45)$$

where k_λ is defined as

$$E_{k_\lambda} = \frac{\hbar^2 k_\lambda^2}{2M} = \frac{\hbar^2 k_0^2}{2M} - \hbar\omega_\lambda \quad (46)$$

and $\hbar\omega_\lambda$ is the excitation energy. \mathbf{k}_λ is the vector $\mathbf{k}_\lambda = k_\lambda \mathbf{r}/r$.

For excitation energies $\hbar\omega_\lambda \ll E_{k_\lambda}$, one obtains the useful relation

$$k_\lambda = (k_0^2 - 2M\omega_\lambda/\hbar)^{1/2} \cong k_0 \left(1 - \frac{M\omega_\lambda}{\hbar k_0^2} \right) \quad (47)$$

or

$$\Delta k = k_\lambda - k_0 = \frac{\omega_\lambda}{v} \quad (48)$$

where v is the projectile velocity.

From 18 the scattering amplitude is given by

$$f_{\lambda\mu}(\theta) = -\frac{M}{2\pi\hbar^2} \langle \mathbf{k}_\lambda | T_{\lambda\mu} | \mathbf{k}_0 \rangle \quad (49)$$

The differential cross section for inelastic scattering is given by

$$\frac{d\sigma_{\lambda\mu}(\theta)}{d\Omega} = \frac{k_\lambda}{k_0} |f_{\lambda\mu}(\theta)|^2 = \left(\frac{M}{2\pi\hbar^2} \right)^2 \frac{k_\lambda}{k_0} |\langle \mathbf{k}_\lambda | T_{\lambda\mu} | \mathbf{k}_0 \rangle|^2 \quad (50)$$

For collective excitations the projectile induces small deformations of the target surface. The matter density of the target will be slightly deformed by an additional term (proportional to the derivative of the ground state density. This term is peaked at the target surface. Since microscopically the interaction potential U_{int} can be regarded as a folding of the nucleon-nucleon interaction and the matter densities, one expects that U_{int} is also peaked at the target surface. This carries the spirit of the Bohr-Mottelson model for collective vibrations. The approximation is valid for light projectiles, mainly proton, α 's, C, O, etc.

In this model, the optical potential is not spherically symmetric, but is slightly deformed. The equipotential surfaces of this field $U_\alpha(r)$ are given by Eq. ??, i.e.,

$$r_\theta = r \left\{ 1 + \sum_{\lambda\mu} \alpha_{\lambda\mu}^* Y_{\lambda\mu}(\hat{\mathbf{r}}) \right\} \quad (51)$$

for constant r . In other words,

$$U_\alpha(r_\theta, \theta) = U_0(r) \quad (52)$$

where $U_0(r)$ is the non-deformed field. Conversely,

$$\begin{aligned} U_\alpha(r, \theta) &= U_0 \left(\frac{r}{1 + \sum_{\lambda\mu} \alpha_{\lambda\mu}^* Y_{\lambda\mu}(\hat{\mathbf{r}})} \right) \\ &= U_0(r) - r \frac{dU_0(r)}{dr} \sum_{\lambda\mu} \alpha_{\lambda\mu}^* Y_{\lambda\mu}(\hat{\mathbf{r}}) + \mathcal{O}(\alpha^2) \end{aligned} \quad (53)$$

Thus, the residual interaction is given by

$$U_{\text{int}} = -r \frac{dU_0(r)}{dr} \sum_{\lambda\mu} \alpha_{\lambda\mu}^* Y_{\lambda\mu}(\hat{\mathbf{r}}) \cong -R_0 \frac{dU_0(r)}{dr} \sum_{\lambda\mu} \alpha_{\lambda\mu}^* Y_{\lambda\mu}(\hat{\mathbf{r}}) \quad (54a)$$

where R_0 is the peak position of $dU_0(r)/dr$.

Thus, for isoscalar excitations we can write ($\lambda \geq 2$)

$$f_{\lambda\mu}^{IS}(\theta) = \frac{M}{2\pi\hbar^2} \langle \Psi_{\lambda\mu} | \alpha_{\lambda\mu}^* | \Psi_0 \rangle R_0 \left\langle \phi_{\mathbf{k}}^{(-)} \left| \frac{dU_0(r)}{dr} Y_{\lambda\mu}(\hat{\mathbf{r}}) \right| \phi_{\mathbf{k}_0}^{(+)} \right\rangle \quad (55)$$

We can rewrite it as

$$f_{\lambda\mu}^{IS}(\theta) = \frac{M}{2\pi\hbar^2} \frac{1}{\sqrt{2\lambda+1}} \delta_\lambda \left\langle \phi_{\mathbf{k}}^{(-1)} \left| \frac{dU_0(r)}{dr} Y_{\lambda\mu}(\hat{\mathbf{r}}) \right| \phi_{\mathbf{k}_0}^{(+)} \right\rangle \quad (56)$$

where δ_λ is the deformation parameter for the nuclear excitation.

The monopole $|0\rangle \rightarrow |\lambda=0\rangle$ transition amplitude is given by

$$f_0(\theta) = \frac{M}{2\pi\hbar^2} \alpha_0 \left\langle \phi_{\mathbf{k}}^{(-)} \left| \left(3U_0(r) + r \frac{dU_0(r)}{dr} \right) Y_{00} \right| \phi_{\mathbf{k}_0} \right\rangle \quad (57)$$

Assuming charge independence of the nuclear interaction, the isovector excitations by the projectile nuclear field arise when the target has a number of protons which is different from that of the neutrons.

From Eq. 54a the surface potential which induces isovector excitations is given by

$$-R_n \frac{dU_0^{(n)}}{dr} \sum_{\lambda\mu} \alpha_{\lambda\mu}^{(n)*} Y_{\lambda\mu}(\hat{\mathbf{r}}) - R_p \frac{dU_0^{(p)}}{dr} \sum_{\lambda\mu} \alpha_{\lambda\mu}^{(p)*} Y_{\lambda\mu}(\hat{\mathbf{r}}) \quad (58)$$

Center of mass correction imply that

$$d_{\lambda\mu}^{(n)} \equiv R_n \alpha_{\lambda\mu}^{(n)*} Y_{\lambda\mu}(\hat{\mathbf{r}}) = Z \left(-\frac{1}{A}\right)^\lambda R \alpha_{\lambda\mu}^* Y_{\lambda\mu}(\hat{\mathbf{r}})$$

$$d_{\lambda\mu}^{(p)} \equiv R_p \alpha_{\lambda\mu}^{(p)} Y_{\lambda\mu}(\hat{\mathbf{r}}) = \left[\left(1 - \frac{1}{A}\right)^\lambda + (-1)^\lambda \frac{(Z-1)}{A^\lambda} \right] R \alpha_{\lambda\mu}^* Y_{\lambda\mu}(\hat{\mathbf{r}}) \quad (59)$$

where $d^{(n)}$ ($d^{(p)}$) is the vibrational amplitude of the neutron (proton) fluid. R is the mean radius of the total (proton + neutron) density.

The isovector potential becomes

$$-R \sum_{\lambda\mu} \alpha_{\lambda\mu}^* Y_{\lambda\mu}(\hat{\mathbf{r}}) \left\{ \overbrace{Z \left(-\frac{1}{A}\right)^\lambda}^{Q_\lambda^{(n)}} \frac{dU_0^{(n)}}{dr} + \left[\overbrace{\left(1 - \frac{1}{A}\right)^\lambda + (-1)^\lambda \frac{Z-1}{A^\lambda}}^{Q_\lambda^{(p)}} \right] \frac{dU_0^{(p)}}{dr} \right\} \quad (60)$$

Note that if $U_0^{(n)} = U_0^{(p)}$ and $Q_\lambda^{(p)} = -Q_\lambda^{(n)}$ there will be no isovector excitations.

If the radii of the neutron and proton potentials are slightly different

$$U_0^{(n)} = U_0(r + R - R_n) \cong U_0(r) + (R - R_n) \frac{dU_0(r)}{dr}$$

$$U_0^{(p)} = U_0(r + R - R_p) \cong U_0(r) + (R - R_p) \frac{dU_0(r)}{dr}$$

where $U_0(r)$ is a mean potential with mean radius R .

Inserting 60 into 58 the isovector potential becomes

$$\Delta U = -R \sum_{\lambda\mu} \alpha_{\lambda\mu}^* Y_{\lambda\mu}(\hat{\mathbf{r}}) \left\{ \left(Q_\lambda^{(n)} + Q_\lambda^{(p)} \right) \left[\frac{dU_0}{dr} + R \frac{d^2 U_0}{dr^2} \right] - \left(Q_\lambda^{(n)} R_n + Q_\lambda^{(p)} R_p \right) \frac{d^2 U_0(r)}{dr^2} \right\}$$

$$\cong -R \sum_{\lambda\mu} \alpha_{\lambda\mu}^* Y_{\lambda\mu}(\hat{\mathbf{r}}) \left(Q_\lambda^{(n)} + Q_\lambda^{(p)} \right) \frac{dU_0}{dr} \quad (61)$$

Thus, for isovector excitations,

$$f_{\lambda\mu}^{IV}(\theta) = \frac{M}{2\pi\hbar^2} \frac{1}{\sqrt{2\lambda+1}} \delta_\lambda \left(Q_\lambda^{(n)} + Q_\lambda^{(p)} \right) \left\langle \phi_k^{(-)} \left| \frac{dU_0}{dr} Y_{\lambda\mu}(\hat{\mathbf{r}}) \right| \phi_{\mathbf{k}0}^{(+)} \right\rangle \quad (62)$$

If we now use the eikonal approximation, $\phi_{\mathbf{k}}^{(-)*}(\mathbf{r}) \phi_{\mathbf{k}0}^{(+)}(\mathbf{r}) \cong e^{i\mathbf{q}\cdot\mathbf{r}+i\chi(b)}$, the integrals in Eqs. 56, 57 and 62 become

$$I_{\lambda\mu} = \int d^3r F_\lambda(r) Y_{\lambda\mu}(\hat{\mathbf{r}}) e^{i\mathbf{q}\cdot\mathbf{r}+i\chi(b)} \quad (63)$$

where

$$F_\lambda(r) = \begin{cases} 3U_0 + r \frac{dU_0}{dr} & , \quad \lambda = 0 \\ \frac{dU_0}{dr} & , \quad \lambda > 0 \end{cases} \quad (64)$$

Using

$$Y_{\lambda\mu}(\hat{\mathbf{r}}) = \sqrt{\frac{2\lambda+1}{4\pi}} \sqrt{\frac{(\lambda-\mu)!}{(\lambda+\mu)!}} P_{\lambda\mu}(\cos\theta) e^{i\mu\phi} \quad (65)$$

and

$$\int d\phi e^{iq_t b \cos\phi + i\mu\phi} = 2\pi i^\mu J_\mu(q_t b) \quad (66)$$

we can write 63 as

$$\begin{aligned} I_{\lambda\mu} &= \sqrt{\pi(2\lambda+1)} \sqrt{\frac{(\lambda-\mu)!}{(\lambda+\mu)!}} i^\mu \int_0^\infty db b J_\mu(q_t b) e^{i\chi(b)} \\ &\times \int_{-\infty}^\infty P_{\lambda\mu}\left(\frac{z}{\sqrt{b^2+z^2}}\right) F_\lambda(b, z) e^{iq_\ell z} dz \end{aligned} \quad (67)$$

where (see Eq. 46)

$$q_\ell = k_0 - k_\lambda \cos\theta \cong k_0 - k_\lambda \cong \frac{\omega\lambda}{v} \quad \text{and} \quad q_t \cong 2\sqrt{k_0 k_\lambda} \sin\frac{\theta}{2}, \quad (68)$$

where θ is the scattering angle and we use the mean wavenumber $\langle k \rangle = \sqrt{k_0 k_\lambda}$ to compute q_t .

Thus, to compute the inelastic scattering amplitudes in the deformed potential model + eikonal approximation one needs to calculate two simple integrals. The scattering amplitudes will depend on the optical potential parameters and on deformation parameters δ_λ and α_0 .

6 Inelastic scattering of exotic nuclei

As we have seen the deformed potential model is based on the surface peaked assumption for the transition density. Although this assumption is reasonable for the excitation of heavy nuclei (e.g., ^{40}Ca , ^{208}Pb , etc.), it is rather crude for light nuclei, especially when the transition density extends radially beyond the nuclear size. This is the case for the soft multipole excitations, for which the transition densities have very long tails, as shown in Fig. 5(a).

The transition strengths were calculated [14] by using the self-consistent HF + RPA method [26]. The dominant peaks of all multipoles appear at $E_x = 1 - 1.5$ MeV, having a narrow width of $\Gamma_{FWHM} \leq 1$ MeV. The transition strengths for the soft modes are calculated to be $B(E0) = 61.4 e^2 \text{ fm}^4$, $B(E1) = 0.82 e^2 \text{ fm}^2$ and $B(E2) = 31.5 e^2 \text{ fm}^4$, respectively, exhausting 11%, 2% and %7 of the EWSR (*Energy Weighted Sum Rule*) values. Although the fraction of the EWSR is small, the transitions

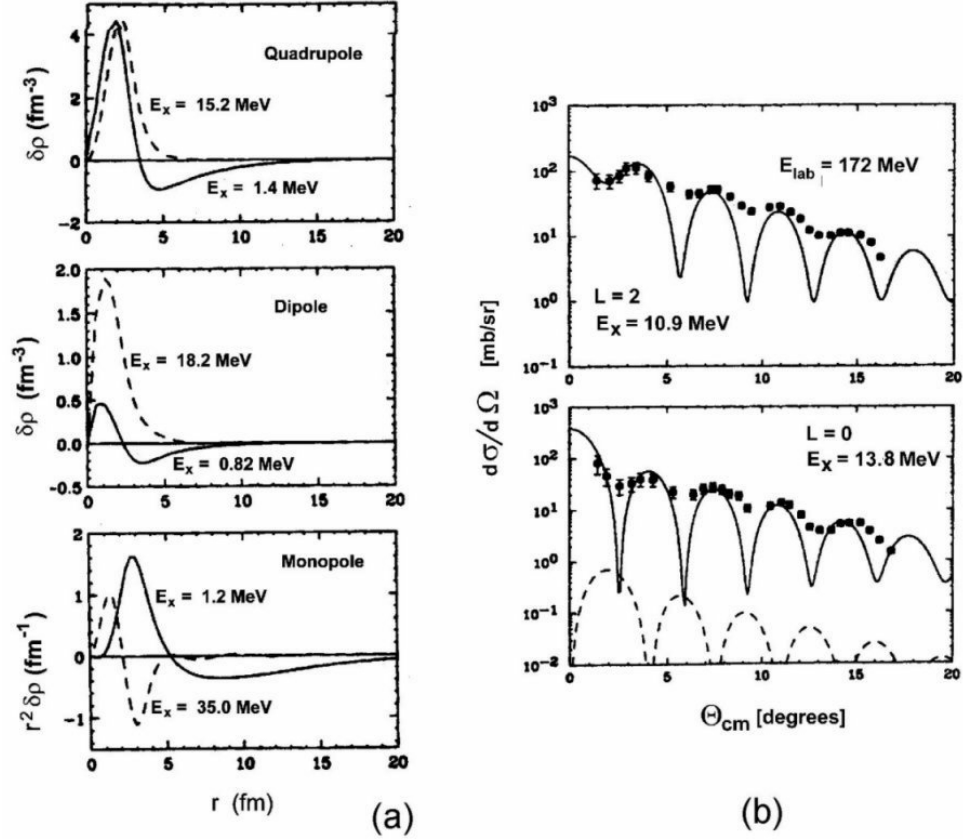


Figure 5 (a) The transition strengths for monopole, dipole and quadrupole excitations in ^{11}Li . (b) Differential cross sections of monopole and quadrupole resonances in ^{208}Pb excited by an α -projectile at $E_{lab} = 172$ MeV.

strengths of the soft multipoles are larger than those of the giant resonances in the same nucleus, because of the very low excitation energies of the soft modes.

In order to test the validity of the formulas developed in the last Sections a calculation of the differential cross sections of monopole and quadrupole resonances in ^{208}Pb excited by an α -projectile at $E_{lab} = 172$ MeV is shown in Fig. 5(b) [14]. The transition densities of both states are calculated by using the HF density of ^{208}Pb and assuming 100% of the energy-weighted sum rules. It is remarkable that both the angular distributions and the absolute magnitudes of the cross sections at forward angles, $\Theta_{cm} \geq 15^\circ$, are well described by using the established optical potentials for the nucleon-nucleus scattering.

We now consider the $^{11}\text{Li} - ^{12}\text{C}$ reaction at $E_{lab} = 30$ and 60 MeV/nucleon. The parameters of the Gaussian potential in Eq. 70 at 30 MeV are $v_0 = 43.9$ MeV, $\omega_0 = 3.29$ MeV, and $a = 2.93$ fm for neutrons and $v_0 = 44.9$ MeV, $\omega_0 = 2.88$ MeV, and $a = 2.93$ fm for protons. At 60 MeV, very similar values [14] were taken. The calculated differential cross sections are shown in Figure 6.

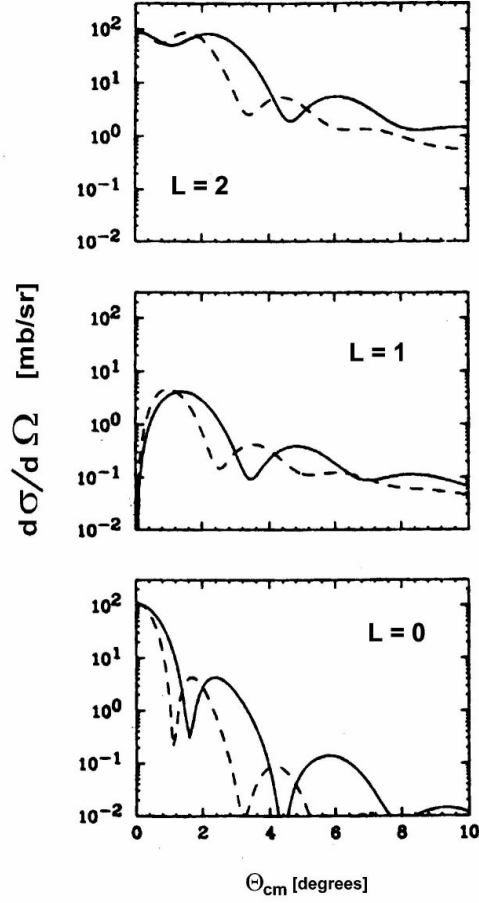


Figure 6 Multipole excitations in ^{11}Li interacting with ^{12}C targets..

There are substantial differences between the monopole and the quadrupole excitations. The first crucial point is the steeper slope of the monopole cross section at very forward angle, $\theta \sim 0^\circ$; the difference is clearly seen in the ratio between the first and second peaks of the cross sections, which is almost 1 for $L = 2$ but than 10 for $L = 0$.

To understand this we observe that, due to the term e^{-z^2/a^2} in the integrand of Eq. 74, that integral is dominated for $z \simeq 0$ values. Thus, $\mathcal{O}_{\lambda\mu} \propto P_{\lambda\mu}(0)$. But $P_{\lambda\mu}(0) = 0$, unless $\lambda + \mu = \text{even}$. Thus three Legendre polynomials with different μ contribute to the cross section in the $L = 2$ case, while only one appears in the $L = 0$ case.

The first deep minimum for the $L = 0$ case is found at $\theta \cong 1.6$ (1.0) $^\circ$ while a shallow appears at $\theta \cong 1.0$ (0.7) $^\circ$ for the $L = 2$ case at $E_{\text{lab}} = 330$ (660) MeV. These differences were certainly an important clue in finding the giant monopole states in many heavy nuclei [25]. It is expected that they play the same role for the inelastic scattering of exotic nuclei.

For $E_{\text{lab}} = 660$ MeV the dips of all multipole excitations occur in shorter intervals because of the larger wave number.

It is interesting to compare the results of Figs. 5(b) and 6. Since the surface is sharp in ^{208}Pb , the slope decreases very slowly in the case of $^{208}\text{Pb} + \alpha$, while it drops quickly in the $^{12}\text{C} + ^{11}\text{Li}$ case because of the very diffuse surface of ^{11}Li . It should be noticed that the absolute magnitude of the differential cross section in Fig. 6 is of the order of 100 mb/sr for the monopole and quadrupole excitations which is almost the same as observed magnitude of the $\text{Pb} + \alpha$ reaction in Fig. 5(b). It is also seen that the soft dipole mode has a smaller cross section and a different angular dependence than those of the other two multipoles. Although a secondary beam always has lower intensity than ordinary beams, the soft multipole excitations could be tested experimentally with modern high sensitivity detector systems.

Supplement C

7 The folding potential model

From Eq. 45 we can write the transition matrix element as

$$T_{\lambda\mu} = \int d^3R \int d^3r \phi_{\mathbf{k}}^{(-)*}(\mathbf{R}) U_{\text{int}}(|\mathbf{R} - \mathbf{r}|) \delta\rho_{\lambda\mu}(\mathbf{r}) \phi_{\mathbf{k}_0}^{(+)}(\mathbf{R}) \quad (69a)$$

where $\delta\rho_{\lambda\mu} = \psi_{\lambda\mu}^* \psi_0$ is the transition density. Instead of using the deformed potential model we can think of $U_{\text{int}}(|\mathbf{R} - \mathbf{r}|)$ as the potential between each nucleon and the projectile. That is, the transition $|0\rangle \rightarrow |\lambda\mu\rangle$ is caused by the (target-nucleon) - projectile interaction.

For simplicity, we shall use a Gaussian form for the (target-nucleon) - projectile potential. This form is reasonable for α , carbon or an oxygen projectile. A Gaussian potential can be easily expanded into multipoles

$$\begin{aligned} U_{\text{int}} &= (v_0 + i\omega_0) e^{-(\mathbf{R}-\mathbf{r})/a^2} = (v_0 + i\omega_0) e^{-(R^2+r^2)/a^2} e^{-\mathbf{R}\cdot\mathbf{r}/a^2} \\ &= 4\pi (v_0 + i\omega_0) e^{-(R^2+r^2)/a^2} \sum_{\lambda\mu} i^\lambda j_\lambda \left(2i \frac{rR}{a^2}\right) Y_{\lambda\mu}(\hat{\mathbf{R}}) Y_{\lambda\mu}^*(\hat{\mathbf{r}}) \end{aligned} \quad (70)$$

Inserting this into Eq. 69a and using the eikonal approximation we get

$$\begin{aligned} T_{\lambda\mu} &= 4\pi (v_0 + i\omega_0) \sum_{\lambda\mu} i^\lambda \int d^3R e^{i\mathbf{q}\cdot\mathbf{r} + i\chi(b)} \\ &\quad \times e^{-R^2/a^2} Y_{\lambda\mu}(\hat{\mathbf{R}}) \int d^3r \delta\rho_{\lambda\mu}(\mathbf{r}) e^{-r^2/a^2} j_\lambda \left(2i \frac{rR}{a^2}\right) Y_{\lambda\mu}(\hat{\mathbf{r}}) \end{aligned} \quad (71)$$

Using Eq. 66 we get ($\mathbf{R} \equiv (\mathbf{b}, z)$)

$$\begin{aligned} T_{\lambda\mu} &= 8\pi^2 (v_0 + i\omega_0) \sum_{\lambda\mu} i^{\lambda+\mu} \int db b J_\mu(qtb) e^{i\chi(b)} \\ &\quad \times e^{-b^2/a^2} \int_{-\infty}^{\infty} dz e^{-z^2/a^2 + i\omega_\lambda z/v} Y_{\lambda\mu}(\theta(z, b), 0) \\ &\quad \times \int d^3r e^{-r^2/a^2} j_\lambda \left(2i \frac{rR}{a^2}\right) \delta\rho_{\lambda\mu}(\mathbf{r}) Y_{\lambda\mu}^*(\hat{\mathbf{r}}) \end{aligned}$$

Or, using $\delta\rho_{\lambda\mu}(\mathbf{r}) \equiv \delta\rho_{\lambda\mu}(r) Y_{\lambda\mu}(\hat{r})$, and Eq. 65,

$$\begin{aligned} T_{\lambda\mu} &= 2\pi\sqrt{4\pi} (v_0 + i\omega_0) \sum_{\lambda\mu} i^{\lambda+\mu} \sqrt{2\lambda+1} \sqrt{\frac{(\lambda-\mu)!}{(\lambda+\mu)!}} \\ &\quad \times \int_0^\infty db b J_\mu(qtb) e^{i\chi(b)} F_{\lambda\mu}(b) \end{aligned} \quad (72)$$

where

$$F_{\lambda\mu}(b) = e^{-b^2/a^2} \int_0^\infty dr r^2 \delta\rho_\lambda(r) \mathcal{O}_{\lambda\mu}(r, b) e^{-r^2/a^2} \quad (73)$$

and

$$\mathcal{O}_{\lambda\mu}(r, b) = \int_{-\infty}^\infty dz e^{-z^2/a^2} j_\lambda \left(2i \frac{rR}{a^2} \right) \rho_{\lambda\mu} \left(\frac{z}{\sqrt{z^2 + b^2}} \right) e^{i\omega_\lambda z/v} \quad (74)$$

Given the parameters v_0, ω_0 and a of the nucleon-projectile potential and the transition density $\delta\rho_\lambda(r)$, Eq. 72 together with Eq. 49 allows us to calculate the inelastic scattering amplitude $f_{\lambda\mu}(\theta)$.

A link between the deformed potential model and the folding model is obtained by using the standard vibrational model. We can write

$$\delta\rho_\lambda = - \begin{cases} \frac{\delta_\lambda}{\sqrt{2\lambda+1}} \frac{d\rho_o}{dr} & \text{for } \lambda \geq 1 \\ \alpha_0 \left(3\rho_0 + r \frac{d\rho_0}{dr} \right) & \text{for } \lambda = 0 \end{cases} \quad (75)$$

As in the deformed potential model, the scattering amplitude is determined by the optical potential parameters and the deformation parameters δ_λ and α_0 . Isovector excitation are obtained by multiplying the above densities by $Q_\lambda^{(n)} + Q_\lambda^{(p)}$ (see Eq. 60).

Another commonly used model for $\delta\rho_\lambda$ is the *Tassie Model* [24] which is given

$$\delta\rho_\lambda(r) = - \frac{\delta_\lambda}{\sqrt{2\lambda+1}} \left(\frac{r}{R_0} \right)^{\lambda-1} \frac{d\rho_0}{dr}, \quad \lambda \geq 1. \quad (76)$$

where R_0 is the nuclear radius. For $\lambda = 0$, one can use 75. In general, both models yield basically the same transition density for heavy nuclei and low lying collective states. The Tassie model is a variant of the standard vibrational model and is more frequently used than the former (also known as the *Bohr-Mottelson Model*).

8 Charge-exchange reactions with radioactive beams

Charge exchange reactions, i.e. (p, n) , (n, p) reactions, are an important tool in nuclear structure physics, providing a measure of the Gamow-Teller strength function in the nuclear excitation spectrum (for a review see, e.g., [27]). Experiments with heavy-ion charge-exchange reactions like $({}^6\text{Li}, {}^6\text{He})$, $({}^{12}\text{C}, {}^{12}\text{N})$, or $({}^{12}\text{C}, {}^{12}\text{B})$ are common [28, 29], one of the advantages being that both initial and final states involve charged particles, so that a better resolution can often be achieved.

But, apart from this aspect, heavy-ion charge-exchange reactions can help us to understand the underlying nature of the exchange mechanism. On microscopic grounds charge exchange is accomplished through charged meson exchange, mainly π - and ρ -exchange. It is well known that neutron-proton scattering at backward angles results from small angle (low momentum transfer) charge-exchange, and is one of the main pieces of evidence for the pion exchange picture of the nuclear force. The width of the peak is roughly given by the exchanged pion momentum divided by the beam

momentum. Therefore, a similar enhancement in the 180 degree elastic scattering of nuclei should be seen in charge exchange between mirror pairs of nuclei.

Charge exchange between mirror nuclei is particularly interesting because at small angles the exchange has zero momentum transfer. Looking at forward angles also has the advantage of eliminating competing processes, namely proton-neutron transfer. Another important advantage of mirror nuclei charge-exchange over (p, n) reactions is that the strong absorption of heavy ions selects large impact parameters and therefore emphasizes the longest range part of the charge exchange force.

In this Section we present a simple description of charge exchange reactions at intermediate and high energy in terms the microscopic π - and ρ -exchange potentials, as developed by Bertulani and collaborators [30]. The eikonal approach to the nucleus-nucleus scattering is used.

The differential cross section for inelastic scattering in a single-particle model is given by

$$\frac{d\sigma}{d\Omega} = \frac{k'}{k} \left(\frac{\mu}{4\pi^2 \hbar^2} \right)^2 (2j_P + 1)^{-1} (2j_T + 1)^{-1} \sum_{\nu, \mathbf{m}} \left| \int_0^\infty db b J_\nu(Q_t b) M(\mathbf{m}, \nu, b) e^{i\chi(b)} \right|^2, \quad (77)$$

where

$$M(\mathbf{m}, \nu, b) = \int_0^\infty dq_t q_t J_\nu(q_t b) \int_0^{2\pi} d\phi_q e^{-i\nu\phi_q} \mathcal{M}(\mathbf{m}, \mathbf{q}) \quad (78)$$

$$\mathcal{M}(\mathbf{m}, \mathbf{q}) = \langle \Phi_f^P(\mathbf{r}_P) \Phi_f^T(\mathbf{r}_T) | e^{-i\mathbf{q}\cdot\mathbf{r}_P} V(\mathbf{q}) e^{i\mathbf{q}\cdot\mathbf{r}_T} | \Phi_i^P(\mathbf{r}_P) \Phi_i^T(\mathbf{r}_T) \rangle, \quad (79)$$

and $\mathbf{m} = (m_T, m'_T, m_P, m'_P)$ is the set of angular momentum quantum numbers of the projectile and target wavefunction. \mathbf{m} is measured along the beam axis, and the subindices T and P refer to the target and projectile, respectively.

We also saw that the probability of one-boson-exchange at the impact parameter b and is given by

$$\overline{\mathcal{P}}(b) = \frac{k'}{k} \left(\frac{1}{4\pi^2 \hbar v} \right)^2 (2j_P + 1)^{-1} (2j_T + 1)^{-1} \exp\{-2 \text{Im} \chi(b)\} \sum_{\nu, \mathbf{m}} |M(\mathbf{m}, \nu, b)|^2, \quad (80)$$

where $\text{Im}\chi(b)$ is the imaginary part of the eikonal phase.

Equations 77 and 80 are the basic results of the eikonal approach to the description of heavy-ion charge-exchange reactions at intermediate and high energies. They can also be used for the calculation of the excitation of Δ particles in nucleus-nucleus peripheral collisions. The essential quantity to proceed further is the matrix element given by Eq. 79 which is needed to calculate the impact-parameter-dependent amplitude $M(\mathbf{m}, \nu, b)$ through Eq. 78. The magnitude of this amplitude decreases with the decreasing overlap between the nuclei, i.e. with the impact parameter b . At small impact parameters the strong absorption will reduce the charge-exchange probability. Therefore, we expect that the probability given by Eq. 80 is peaked at the grazing impact parameter.

Supplement D

9 Pion- and rho-exchange between projectile and target nucleons

In momentum representation the pion+rho exchange potential is given by

$$V(\mathbf{q}) = -\frac{f_\pi^2}{m_\pi^2} \frac{(\boldsymbol{\sigma}_1 \cdot \mathbf{q})(\boldsymbol{\sigma}_2 \cdot \mathbf{q})}{m_\pi^2 + \mathbf{q}^2} (\boldsymbol{\tau}_1 \cdot \boldsymbol{\tau}_2) - \frac{f_\rho^2}{m_\rho^2} \frac{(\boldsymbol{\sigma}_1 \times \mathbf{q}) \cdot (\boldsymbol{\sigma}_2 \times \mathbf{q})}{m_\rho^2 + \mathbf{q}^2} (\boldsymbol{\tau}_1 \cdot \boldsymbol{\tau}_2), \quad (81)$$

where the pion (rho) coupling constant is $f_\pi^2/4\pi = 0.08$ ($f_\rho^2/4\pi = 4.85$), $m_\pi c^2 = 145$ MeV, and $m_\rho c^2 = 770$ MeV.

The central part of the potential above has a zero-range component, which is a consequence of the point-like treatment of the meson-nucleon coupling. In reality the interaction extends over a finite region of space, so that the zero range force must be replaced by an extended source function. This can be done by adding a short-range interaction defined at $q = 0$ in terms of the *Landau-Migdal parameters* g'_π and g'_ρ . We will use $g'_\pi = 1/3$ and $g'_\rho = 2/3$, which amounts to remove exactly the zero-range interaction (for details, see, e.g., [27]).

Since the ρ -exchange interaction is of very short-range, its central part is appreciably modified by the ω -exchange force. The effect of this repulsive correlation is approximated by multiplying V_ρ^{cent} by a factor $\xi = 0.4$ and leaving V_ρ^{tens} unchanged since the tensor force is little affected by ω -exchange [32].

With these modifications the pion+rho exchange potential can be written as

$$V(\mathbf{q}) = V_\pi(\mathbf{q}) + V_\rho(\mathbf{q}) = \left[v(\mathbf{q})(\boldsymbol{\sigma}_1 \cdot \hat{\mathbf{q}})(\boldsymbol{\sigma}_2 \cdot \hat{\mathbf{q}}) + w(\mathbf{q})(\boldsymbol{\sigma}_1 \cdot \boldsymbol{\sigma}_2) \right] (\boldsymbol{\tau}_1 \cdot \boldsymbol{\tau}_2), \quad (82)$$

where

$$v(\mathbf{q}) = v_\pi^{tens}(\mathbf{q}) + v_\rho^{tens}(\mathbf{q}), \quad (83)$$

and

$$w(\mathbf{q}) = w_\pi^{cent}(\mathbf{q}) + \xi w_\rho^{cent}(\mathbf{q}) + w_\pi^{tens}(\mathbf{q}) + w_\rho^{tens}(\mathbf{q}), \quad (84)$$

with

$$v_\pi^{tens}(\mathbf{q}) = -J_\pi \frac{\mathbf{q}^2}{m_\pi^2 + \mathbf{q}^2}, \quad v_\rho^{tens}(\mathbf{q}) = J_\rho \frac{\mathbf{q}^2}{m_\rho^2 + \mathbf{q}^2} \quad (85)$$

$$w_\pi^{cent}(q) = -\frac{1}{3} J_\pi \left[\frac{\mathbf{q}^2}{m_\pi^2 + \mathbf{q}^2} - 3g'_\pi \right], \quad w_\rho^{cent}(q) = -\frac{2}{3} J_\rho \left[\frac{\mathbf{q}^2}{m_\rho^2 + \mathbf{q}^2} - \frac{3}{2} g'_\rho \right] \quad (86)$$

$$w_\pi^{tens}(q) = \frac{1}{3} J_\pi \frac{\mathbf{q}^2}{m_\pi^2 + \mathbf{q}^2}, \quad w_\rho^{tens}(q) = -\frac{1}{3} J_\rho \frac{\mathbf{q}^2}{m_\rho^2 + \mathbf{q}^2}. \quad (87)$$

The values of the coupling constants J_π and J_ρ in nuclear units are given by

$$\begin{aligned} J_\pi &= \frac{f_\pi^2}{m_\pi^2} \equiv f_\pi^2 \frac{(\hbar c)^3}{(m_\pi c^2)^2} \simeq 400 \text{ MeV fm}^3 \\ J_\rho &= \frac{f_\rho^2}{m_\rho^2} \equiv f_\rho^2 \frac{(\hbar c)^3}{(m_\rho c^2)^2} \simeq 790 \text{ MeV fm}^3 \end{aligned} \quad (88)$$

Turning off the terms $w_{\pi,\rho}^{cent}$, or $v_{\pi,\rho}^{tens}$ and $w_{\pi,\rho}^{tens}$, allows us to study the contributions from the central and the tensor interaction, and from π - and ρ -exchange, respectively.

Using Eq. 82, single-particle wavefunctions, $\phi_{j\ell m}$, and the representations

$$\begin{aligned}\boldsymbol{\tau}_P \cdot \boldsymbol{\tau}_T &= \tau_P^0 \tau_T^0 + \tau_P^+ \tau_T^- + \tau_P^- \tau_T^+ \\ \boldsymbol{\sigma}_P \cdot \boldsymbol{\sigma}_T &= \sigma_P^0 \sigma_T^0 + \sigma_T^+ \sigma_P^- + \sigma_P^- \sigma_T^+\end{aligned}$$

yields

$$\begin{aligned}\mathcal{M}(\mathbf{m}, \mathbf{q}) &= w(\mathbf{q}) \sum_{\mu\lambda} \langle \phi_{j\ell m'_T}^{(\pi)} | \sigma_\mu \tau_\lambda e^{i\mathbf{q}\cdot\mathbf{r}_T} | \phi_{j\ell m_T}^{(\nu)} \rangle \langle \phi_{j\ell m'_P}^{(\nu)} | \sigma_\mu \tau_\lambda e^{-i\mathbf{q}\cdot\mathbf{r}_P} | \phi_{j\ell m_P}^{(\pi)} \rangle \\ + v(\mathbf{q}) \sum_{\mu\mu'\lambda} \hat{q}_\mu \hat{q}'_{\mu'} &\langle \phi_{j\ell m'_T}^{(\pi)} | \sigma_\mu \tau_\lambda e^{i\mathbf{q}\cdot\mathbf{r}_T} | \phi_{j\ell m_T}^{(\nu)} \rangle \langle \phi_{j\ell m'_P}^{(\nu)} | \sigma_{\mu'} \tau_\lambda e^{-i\mathbf{q}\cdot\mathbf{r}_P} | \phi_{j\ell m_P}^{(\pi)} \rangle\end{aligned}\quad (89)$$

where

$$\hat{q}_\mu = \sqrt{\frac{4\pi}{3}} Y_{1\mu}(\hat{\mathbf{q}}). \quad (90)$$

Eq. 89 reduces to

$$\begin{aligned}\mathcal{M}(\mathbf{m}, \mathbf{q}) &= w(\mathbf{q}) \sum_{\mu} \langle \phi_{j\ell m'_T} | \sigma_\mu e^{i\mathbf{q}\cdot\mathbf{r}} | \phi_{j\ell m_T} \rangle \langle \phi_{j\ell m'_P} | \sigma_\mu e^{-i\mathbf{q}\cdot\mathbf{r}} | \phi_{j\ell m_P} \rangle \\ + \frac{4\pi}{3} v(\mathbf{q}) \sum_{\mu\mu'} Y_{1\mu}(\hat{\mathbf{q}}) Y_{1\mu'}(\hat{\mathbf{q}}) &\langle \phi_{j\ell m'_T} | \sigma_\mu e^{i\mathbf{q}\cdot\mathbf{r}} | \phi_{j\ell m_T} \rangle \langle \phi_{j\ell m'_P} | \sigma_{\mu'} e^{-i\mathbf{q}\cdot\mathbf{r}} | \phi_{j\ell m_P} \rangle\end{aligned}\quad (91)$$

Expanding $e^{i\mathbf{q}\cdot\mathbf{r}}$ into multipoles we can write

$$\langle \phi_{j\ell m'} | \sigma_\mu e^{i\mathbf{q}\cdot\mathbf{r}} | \phi_{j\ell m} \rangle = 4\pi \sum_{IM} i^I Y_{IM}^*(\hat{\mathbf{q}}) \langle \phi_{j\ell m'} | j_I(qr) Y_{IM}(\hat{\mathbf{r}}) \sigma_\mu | \phi_{j\ell m} \rangle. \quad (92)$$

Since $j_I(qr) Y_{IM}(\hat{\mathbf{r}})$ is an irreducible tensor,

$$\sigma_\mu j_I(qr) Y_{IM}(\hat{\mathbf{r}}) = \sum_{I'M'} (I1M\mu | I'M') \Psi_{I'M'}, \quad (93)$$

where $\Psi_{I'M'}$ is also an irreducible tensor. Therefore,

$$\begin{aligned}\langle \phi_{j\ell m'} | \sigma_\mu j_I(qr) Y_{IM}(\hat{\mathbf{r}}) | \phi_{j\ell m} \rangle &= \sum_{I'M'} (I1M\mu | I'M') \langle \phi_{j\ell m'} | \Psi_{I'M'} | \phi_{j\ell m} \rangle \\ &= \sum_{I'M'} (I1M\mu | I'M') (jI'mM' | jm') \langle \phi_j || \Psi_{I'} || \phi_j \rangle.\end{aligned}\quad (94)$$

The Eqs. 91-94 allows one to calculate the charge-exchange between single-particle orbitals. The quantity needed is the reduced matrix element $\langle \phi_j || [j_I(qr) \sigma \otimes Y_I]_{I'} || \phi_j \rangle$ (see, e.g., [33]). If several orbitals contribute to the process, the respective amplitudes can be added and further on averaged in the cross sections.

10 Low-momentum limit and Gamow-Teller matrix elements

From Eqs. 81-87 we see that the central interaction $w^{cent}(\mathbf{q})$ dominates the low-momentum scattering $\mathbf{q} \sim 0$. In this case, the matrix element 89 becomes

$$\mathcal{M}(i \rightarrow f; \mathbf{q} \sim 0) \sim C_{spins} w^{cent}(\mathbf{q}) \mathcal{M}(GT; P \rightarrow P') \mathcal{M}(GT; T \rightarrow T'), \quad (95)$$

where

$$C_{spins} = \sum_{\mu} \langle I_P M_P 1\mu | I_{P'} M_{P'} \rangle \langle I_T M_T 1\mu | I_{T'} M_{T'} \rangle, \quad (96)$$

and $\mathcal{M}(GT; A \rightarrow A') = \langle A || \sigma\tau || A' \rangle$ are the Gamow-Teller (GT) matrix elements for a particular nuclear transition of the projectile ($A = P$) and of the target ($A = T$).

Inserting 95 into Eq. 78 and using the low-momentum limit, we obtain

$$M(i \rightarrow f; b) \sim C_{spins} w^{(0)} \mathcal{M}(GT; P \rightarrow P') \mathcal{M}(GT; T \rightarrow T') \delta_{\nu 0}, \quad (97)$$

where

$$w^{(0)} = 2\pi \int_0^{q_{cut}} dq q w^{cent}(\mathbf{q}), \quad (98)$$

where q_{cut} is a cutoff-momentum, up to which value the low momentum approximation can be justified.

With these approximations, a general expression can be obtained from Eq. 77,

$$\begin{aligned} \frac{d\sigma}{d\Omega}(\mathbf{q} \sim 0) &= \frac{k'}{k} \left(\frac{\mu}{4\pi^2 \hbar^2} \right)^2 \left[w^{(0)} \right]^2 F(\theta) B(GT; P \rightarrow P') B(GT; T \rightarrow T') \\ &\times \sum_{spins} [C_{spins}]^2 \end{aligned} \quad (99)$$

where

$$B(GT; A \rightarrow A') = |\langle A' || \sigma\tau || A \rangle|^2 \quad (100)$$

is the Gamow-Teller transition density for the nucleus A. The sum over spins includes an average over initial spins and a sum over the final spins of the nuclei.

With these approximations the scattering angular distribution is solely determined by the function

$$F(\theta) = \left| \int db b J_0(kb \sin \theta) e^{i\chi(b)} \right|^2. \quad (101)$$

In the sharp-cutoff limit ($\exp[i\chi(b)] = \Theta(b - R)$), this function reduces to the very simple result

$$F(\theta) = \frac{R^2}{k^2 \sin^2 \theta} J_1^2(kR \sin \theta), \quad (102)$$

which displays a characteristic diffraction pattern.

From the above discussion, we see that the ability to extract information on the Gamow-Teller transition densities in a simple way depends on the validity of

the low-momentum transfer assumption. We shall test this assumption, using the results obtained above, in the special case of the $^{13}\text{C}(^{13}\text{N}, ^{13}\text{C})^{13}\text{N}$ reaction at 70 MeV/nucleon, as reported in Ref. [31].

Supplement E

11 Matrix elements for mirror nuclei

A reasonably good candidate for the investigation of charge-exchange between mirror nuclei is the reaction $^{13}\text{C}(^{13}\text{N}, ^{13}\text{C})^{13}\text{N}$ since ^{13}C targets are now available and a relatively intense ^{13}N beam can be produced [31]. This pair of mirror nuclei is also suitable because the first excited state ($\frac{3}{2}^-$) lies relatively high in energy (3.51 MeV), so that a clear separation can be done between ground-state and excited state transitions. Also, these nuclei have a single nucleon on the $1p_{1/2}$ orbit. Since the reaction is very peripheral, one expects that the charge-exchange process is practically determined by the participation of these valence nucleons. Therefore, this reaction should be a clear probe of charge exchange in a nuclear environment.

One assumes that the pion or rho is exchanged between the neutron in the $1p_{1/2}$ -orbital of ^{13}C and the proton of the $1p_{1/2}$ -orbital of ^{13}N . Configuration mixing is not included for simplicity.

Using Eq. A.2.24 of Ref. [33] one finds

$$\langle p_{1/2} || [j_I(qr) \sigma \otimes Y_I]_{I'} || p_{1/2} \rangle = -\frac{1}{2\sqrt{3}\pi} \begin{cases} \mathcal{F}_0, & \text{if } I=0, I' = 1; \\ 2\sqrt{2} \mathcal{F}_2, & \text{if } I=2, I' = 1; \\ 0 & \text{otherwise,} \end{cases} \quad (103)$$

where

$$\mathcal{F}_I = \int_0^\infty R_{1p_{1/2}}^2(r) j_I(qr) r^2 dr. \quad (104)$$

The above result means that only transitions with $\Delta\ell = 0$ and $\Delta\ell = 2$ in the $1p_{1/2}$ -orbital are allowed. We calculate the radial form factors F_0 and F_2 using harmonic oscillator functions for the $1p_{1/2}$ -orbitals in ^{13}N and ^{13}C :

$$R_{1p_{1/2}}(r) = \left(\frac{8}{3\pi^{1/2}a^5} \right)^{1/2} r e^{-r^2/a^2}, \quad (105)$$

where $a = (\hbar/m_N\omega)^{1/2}$ is the oscillator parameter. For ^{13}C and ^{13}N we take $a = 1.55$ (fm).

We find

$$\mathcal{F}_0 = \left(1 - \frac{q^2 a^2}{6} \right) e^{-q^2 a^2/4}, \quad \text{and} \quad \mathcal{F}_2 = \frac{q^2 a^2}{6} e^{-q^2 a^2/4}. \quad (106)$$

The matrix element 92 becomes

$$\langle \phi_{j\ell m'} | \sigma_\mu e^{\pm i\mathbf{q}\cdot\mathbf{r}} | \phi_{j\ell m} \rangle = \mathcal{C}_0(m, m', \mu) \mathcal{F}_0(q) + \mathcal{C}_2(m, m', \mu, \hat{\mathbf{q}}) \mathcal{F}_2(q), \quad (107)$$

where

$$\mathcal{C}_0(m, m', \mu) = -\frac{1}{\sqrt{3}} (1m, m' - m | m') \delta_{m' - m, \mu} \quad (108)$$

$$\begin{aligned} \mathcal{C}_2(m, m', \mu, \hat{\mathbf{q}}) &= 4\sqrt{\frac{2\pi}{3}} (1m, m' - m | m') (21, m' - m - \mu, \mu | 1, m' - m) \\ &\times Y_{2, m' - m - \mu}^*(\hat{\mathbf{q}}) \end{aligned} \quad (109)$$

Inserting these results in Eq. 91, the integral (78) is easily performed. Using

$$\begin{aligned} Y_{\ell m}(\hat{\mathbf{q}}_t) &= (-1)^{(\ell+m)/2} \left(\frac{2\ell+1}{4\pi} \right)^{1/2} \frac{[(\ell-m)! (\ell+m)!]^{1/2}}{(\ell-m)!! (\ell+m)!!} e^{im\phi}, \quad \text{if } \ell+m = \text{even} \\ &= 0, \quad \text{otherwise,} \end{aligned} \quad (110)$$

and

$$\int_0^{2\pi} e^{i(m-\nu)\phi} d\phi = 2\pi \delta_{m,\nu} \quad (111)$$

and the definition (78), one finds

$$\begin{aligned} M(\mathbf{m}, \nu, b) &= \int_0^\infty dq q J_\nu(qb) \left\{ w [X_{00} \mathcal{F}_0^2(q) + X_{02} \mathcal{F}_0(q) \mathcal{F}_2(q) + X_{22} \mathcal{F}_2^2(q)] \right. \\ &\quad \left. + \frac{4\pi}{3} v(q) [W_{00} \mathcal{F}_0^2(q) + W_{02} \mathcal{F}_0(q) \mathcal{F}_2(q) + W_{22} \mathcal{F}_2^2(q)] \right\}, \end{aligned} \quad (112)$$

where the coefficients X_{ij} and W_{ij} are given in terms of sums of products of \mathcal{C}_0 and \mathcal{C}_2 (see Ref. [30]).

The momentum integral in 112 can be performed numerically. This simple example shows how the magnetic quantum numbers complicate the calculation. The inclusion of other orbits yields a lengthy calculation.

12 Application to $^{13}\text{C} + ^{13}\text{N}$

The method described above was used in Ref. [30] to study the charge-exchange reaction with $^{13}\text{C} + ^{13}\text{N}$ at 70 MeV/nucleon. An optical potential was chosen to fit the reaction $^{12}\text{C} + ^{12}\text{C}$ at 85 MeV/nucleon [13].

Figure 7(a) shows the contributions from π (dashed-curve) and from ρ -exchange (dotted-curve) to the charge exchange probability as a function of the impact parameter. The solid curve is the total probability. The exchange probability is peaked at grazing impact parameters: at low impact parameters the strong absorption makes the probability small, whereas at large impact parameters it is small because of the short-range of the exchange potentials. The value of the exchange probability at the peak is about 1.2×10^{-5} . It is clear from Figure 7(a) that the process is dominated by π -exchange. At small impact parameters the short-range ρ -exchange contribution is large due to a larger overlap between the nuclei.

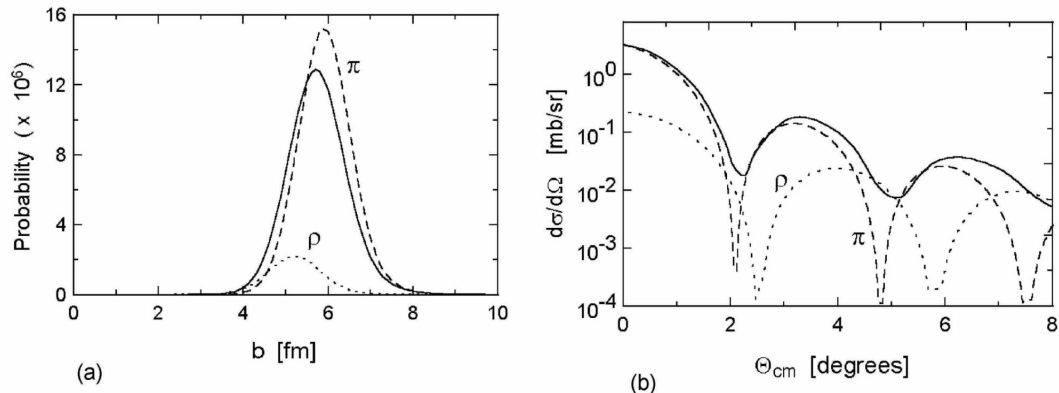


Figure 7 (a) Probability for π - (dashed-curve) and ρ -exchange (dotted-curve) in the reaction $^{13}\text{C}(^{13}\text{N}, ^{13}\text{C})^{13}\text{N}$ at 70 MeV/nucleon, as a function of the impact parameter. The solid curve represents the result of the full interaction. (b) Angular distribution for charge-exchange in the reaction $^{13}\text{C}(^{13}\text{N}, ^{13}\text{C})^{13}\text{N}$ at 70 MeV/nucleon. The contribution from π - (dashed-curve) and ρ -exchange (dotted-curve) are displayed separately. The solid curve represents the result of the full interaction.

In Figure 7(b) the differential cross section is plotted. One observes that at very forward angles the π -exchange contributes to the largest part of the cross section. But ρ -exchange is important at large angles. It has the net effect of smoothing out the dips of the angular distribution. Since π -exchange is of longer range than ρ -exchange, the dips caused by the two contributions are displaced; the ones from ρ -exchange alone are located at larger angles, as expected from the relation $\theta \sim 1/r$. If we put $\mathcal{F}_{0,2} = 1$ and $\exp i\chi(b) = 1$, we obtain that at very small scattering angles the π - and ρ -exchange contributions to the differential cross sections are approximately of the same magnitude. This means that ρ -exchange is more important when distortions are weaker, i.e., in nucleon-nucleon or nucleon-nucleus scattering [27].

The non-spin flip components are strongly suppressed and the cross section is dominated by simultaneous spin-flip components, with $\Delta j = 0$ (33%) and $\Delta j = 2$ (16.8%). This can be understood in terms of the contributions of the tensor and the central part of the pion+rho interaction to the heavy-ion charge-exchange. The central (tensor) force is responsible for the $\Delta j = 0$ (2) transitions.

The total cross section obtained is 7.6 (μb). The peak value of the differential cross section at 0° is 3.5 (mb/sr). These values are of the order of magnitude of the charge-exchange cross sections measured for other systems [29].

Finally, we make a remark on the double exchange reactions. From the values obtained above one sees that the charge exchange probability as a function of impact parameter is small, of order of 10^{-5} . Even for enhanced transitions, one should not expect an increase higher than a factor 10 in the probability. An estimate of double-charge exchange is obtained from Eq. (16), replacing $\mathcal{P}(b)$ by $\mathcal{P}^2(b)/2$. That is, the ratio between the single and the double-charge exchange is of order of $10^{-4} - 10^{-5}$. If the single-step total cross section is of order of tens of microbarns, the double-step

one is of order of nanobarns, in the best cases. Similarly, if the peak of the differential cross section at zero degrees is of order of tens of millibarns, the corresponding one for double-charge exchange will be of order of microbarns, in the best cases. The measurement of double-charge-exchange in heavy-ion collisions therefore requires intense beams and good detection efficiency.

13 References

1. H. Feshbach, *Ann. Phys.* **19** (1962) 287.
2. M.S. Hussein, A.J. Baltz and B.V. Carlson, *Phys. Rep.* **113** (1984).
3. W.G. Love, T. Terasawa and G.R. Satchler, *Phys. Rev. Lett.* **39** (1977) 6; *Nucl. Phys.* **A291** (1977) 183.
4. A.J. Baltz, S.K. Kauffmann, N.K. Glendenning and K. Pruess, *Phys. Rev. Lett.* **40** (1978) 20; *Nucl. Phys.* **A327** (1979) 221.
5. R. Donangelo, L.F. Canto and M.S. Hussein, *Nucl. Phys.* **A320** (1979) 422.
6. R. Donangelo, L.F. Canto and M.S. Hussein, *Phys. Rev.* **C19** (1979) 1801.
7. R.A. Broglia, G. Pollarolo and A. Winther, *Nucl. Phys.* **A361** (1981) 307; **A406** (1983) 369.
8. Fl. Stancu and D.M. Brink, *Phys. Rev.* **C25** (1982) 2450.
9. L.F. Canto, R. Donangelo and M.S. Hussein, *Nucl. Phys.* **A529** (1991) 243.
10. C.A. Bertulani and M.S. Hussein, *Nucl. Phys.* **A524** (1991) 306.
11. L.S. de Paula and L.F. Canto, *Phys. Rev.* **C42** (1990) 2628.
12. *Handbook of Mathematical Functions*, edited by M. Abramowitz and I. Stegun (U.S.GPO, Bureau of Standards, Washington, DC, 1964).
13. M. Buenerd, P. Martin, R. Bertholet, C. Guet, M. Maurel, J. Mougey, H. Nifenecker, J. Pinston, P. Perrin, F. Schlusser, J. Julien, J.P. Bondorf, L. Carlen, H.A. Gustafsson, B. Jakobsson, T. Johansson, P. Kristiansson, O.B. Nielsen, A. Oskarsson, I. Otterlund, H. Ryde, B. Schroeder and G. Tibeli, *Phys. Rev.* **C26** (1982) 1299.
14. C.A. Bertulani and H. Sagawa, *Phys. Lett.* **B300** (1993) 205.
15. S.M. Lenzi, F. Zardi and A. Vitturi, *Phys. Rev.* **C42** (1990) 2079.
16. T. Kobayashi, *Nucl. Phys.* **A538** (1992) 343c.
17. M. Levitowicz et al., *Nucl. Phys.* **A** (1993)
18. C.-B. Moon et al., *Phys. Lett.* **B297** (1992) 39.
19. A.N.F. Aleixo, C.A. Bertulani and M.S. Hussein, *Phys. Rev.* **C43** (1991) 2722.
20. L.F. Canto, R. Donangelo and M.S. Hussein, *Nucl. Phys.* **A529** (1991) 243.
21. J. Barrette et al., *Phys. Lett.* **B209** (1988) 182.
22. G.R. Satchler, K.W. McVoy and M.S. Hussein, *Nucl. Phys.* **A.552** (1991) 621.
23. I.J. Thompson et al., *Phys. Rev.* **C47** (1993) 1364.
24. L.J. Tassie, *Austral. J. Phys.* **9** (1956) 407.
25. H. Morsch et al., *Phys. Rev.* **C28** (1983) 1947
26. G. Bertsch and S.F. Tsai, *Phys. Rep.* **18** (1975) 127.
27. G.F. Bertsch and H. Esbensen, *Rep. Prog. Phys.* **50** (1987) 607.

28. J.S. Winfield, N. Anantaraman, S.M. Austin, L.H. Harwood, J. van der Plicht, H.-L. Wu and A.F. Zeller, Phys. Rev. **C33** (1986) 1333; **35** (1987) 1166(E).
29. N. Anantaraman, J.S. Winfield, S.M. Austin, J.A. Carr, C. Djalali, A. Gilibert, W. Mittig, J.A. Nolen, Jr., and Z.W. Long, Phys. Rev. **C44** (1991) 398.
30. C.A. Bertulani, Nucl. Phys. **A554** (1993) 493; C.A. Bertulani and P. Lotti, Phys. Lett. **B402** (1997) 237; C.A. Bertulani and D. Dolci, Nucl. Phys. **A683** (2001) 635.
31. M. Steiner et al., Phys. Rev. Lett. **76** (1996) 26; Phys. Rev. Lett. **76** (1996) 3042.
32. M.R. Anastasio and G.E. Brown, Nucl. Phys. **A285** (1977) 516.
33. R.D. Lawson, *“Theory of the Nuclear Shell Model”*, Clarendon Press, Oxford, 1980.